

Electronic Structure of UTe_2 Studied by Photoelectron Spectroscopy

Shin-ichi Fujimori^{1*}, Ikuto Kawasaki¹, Yukiharu Takeda¹, Hiroshi Yamagami^{1,2}, Ai Nakamura³, Yoshiya Homma³, and Dai Aoki³

¹Materials Sciences Research Center, Japan Atomic Energy Agency, Sayo, Hyogo 679-5148, Japan

²Department of Physics, Faculty of Science, Kyoto Sangyo University, Kyoto 603-8555, Japan

³Institute for Materials Research, Tohoku University, Oarai, Ibaraki 311-1313, Japan

The electronic structure of the unconventional superconductor UTe_2 was studied by resonant photoelectron spectroscopy (RPES) and angle-resolved photoelectron spectroscopy (ARPES) with soft X-ray synchrotron radiation. The partial U $5f$ density of states of UTe_2 were imaged by the U $4d$ - $5f$ RPES and it was found that the U $5f$ state has an itinerant character, but there exists an incoherent peak due to the strong electron correlation effects. Furthermore, an anomalous admixture of the U $5f$ states into the Te $5p$ bands was observed at a higher binding energy, which cannot be explained by band structure calculations. On the other hand, the band structure of UTe_2 was obtained by ARPES and its overall band structure were mostly explained by band structure calculations. These results suggest that the U $5f$ states of UTe_2 have itinerant but strongly-correlated nature with enhanced hybridization with the Te $5p$ states.

The unconventional superconductivity in f -based materials has attracted much attention over the years. Recently, it was discovered that UTe_2 is one such superconductor with a relatively high transition temperature of $T_{SC} = 1.6$ K.¹⁾ Although its transport properties and the nature of its superconductivity have been extensively studied,²⁾ information on its electronic structure is very limited. In the present study, we have applied U $4d$ - $5f$ resonant photoelectron spectroscopy (RPES)³⁾ and soft x-ray angle-resolved photoelectron spectroscopy (ARPES)⁴⁾ to UTe_2 to unveil its detailed electronic structure.

Photoemission experiments were performed on the soft X-ray beamline BL23SU at SPring-8.⁵⁾ The overall energy resolution in the angle-integrated photoelectron spectroscopy (AIPES) experiments at $h\nu = 800$ eV was about 140 meV and that in the ARPES experiments at $h\nu = 565 - 675$ eV was 90 - 115 meV, depending on the photon energies.

The angular resolution of the ARPES experiments was about $\pm 0.15^\circ$, corresponding to a momentum resolution of about 0.065 \AA^{-1} at $h\nu = 600$ eV. High quality single crystals of UTe_2 were grown using a chemical vapor transport method, as previously described in Ref. 1. A clean sample surface was obtained by cleaving the samples perpendicular to the c axis in an ultra-high vacuum chamber. The positions of the ARPES cuts were determined by assuming a free-electron final state, and the inner potential was taken as $V_0 = 12$ eV. For the ARPES spectra, background contributions from elastically scattered photoelectrons due to surface disorder or phonons were subtracted by assuming momentum-independent spectra.⁶⁾ Note that the AIPES and resonant photoemission (RPES) spectra were recorded from the single crystal surface, and they are the integration of the spectra over the rectangular region with the longer side along

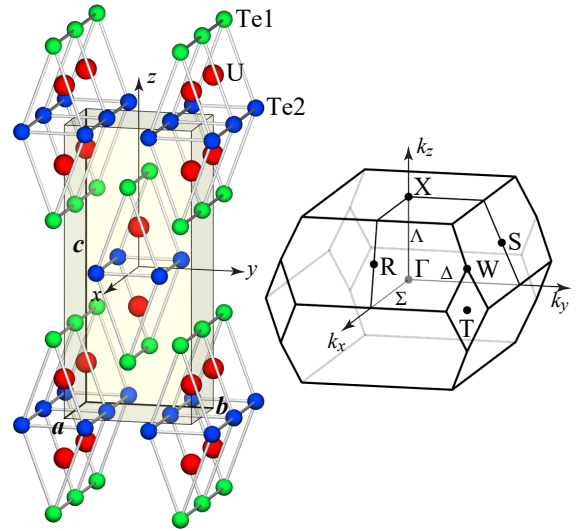


Fig. 1. Crystal structure (left) and Brillouin zone (right) of UTe_2 .

the k_x direction. Although the entire Brillouin zone was not covered, the region includes various portions of the Brillouin zone, and the integrated spectra are enough to be compared with calculated pDOS. The vacuum during the course of the measurements was typically $< 1.5 \times 10^{-8}$ Pa, and the sample surfaces were stable for the duration of the measurements (2 - 3 days). The sample temperature was kept at 20 K for all of the measurements.

Figure 1 shows the crystal structure and Brillouin zone of UTe_2 , which has a body-centered orthorhombic symmetry with $c > b > a$. Note that there are three independent Γ -X high-symmetry lines, namely along the Γ - (Σ) -X, Γ - (Δ) -X, and Γ - (Λ) -X lines corresponding to the k_x , k_y , and k_z directions, respectively. In the present study, the ARPES scans

*fujimori@spring8.or.jp

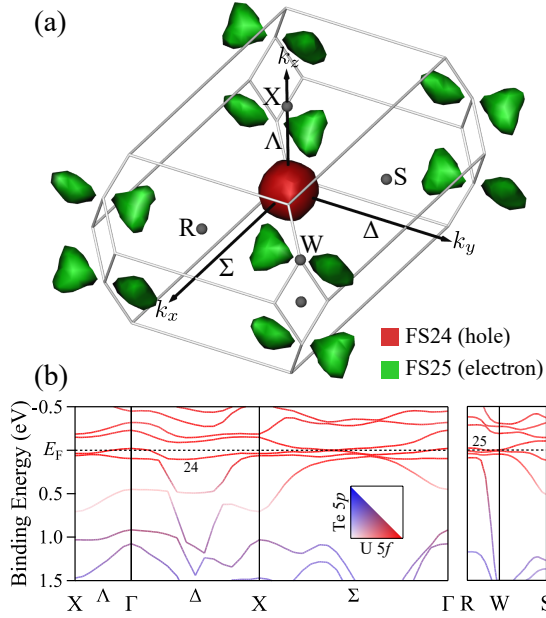


Fig. 2. Calculated Fermi surface and band structure of UTe_2 . (a) Calculated Fermi surface and (b) calculated band structure in the vicinity of E_F . The color coding of each band represents the contributions from the U $5f$ and Te $5p$ states.

were carried out by changing the electron detection angle along the a axis (k_x direction) and the incident photon energy, which correspond to a two dimensional scan within the k_x - k_z plane in the momentum space.

Band structure calculations for UTe_2 were carried out, treating all of the U $5f$ electrons as being itinerant using the relativistic linear augmented plane wave method⁷⁾ within a local density approximation.⁸⁾ Figure 2 (a) shows the calculated Fermi surfaces of UTe_2 . The calculations predict that UTe_2 is a semimetal, consistent with the metallic nature of UTe_2 . Band 24 forms a spherical hole pocket around the Γ point, while band 25 forms a twisted pair of heart-like electron pockets along the R-W-R high-symmetry line. The calculated band structure is shown in Fig. 2 (b), in which the contributions from the U $5f$ and Te $5p$ states are indicated by the color coding of each band. The calculations predicted some less-dispersive bands with large contribution from the U $5f$ states in the very vicinity of the Fermi energy (E_F), forming very shallow electron or hole pockets. For example, the top of band 24 and the bottom of band 25 are about 20 meV above and 8 meV below E_F , respectively. Thus, a tiny change in the Fermi energy drastically transforms the shape of the Fermi surface. This situation is very similar to the case of ferromagnetic heavy Fermion superconductors such as URhGe⁹⁾ and UCoGe.⁶⁾

Figure 3 shows the AIPES spectrum of UTe_2 measured at $h\nu = 800$ eV and the partial density of states (pDOS) obtained from the band structure calculations. The spectrum has a sharp peak structure just below the E_F and long tail toward higher binding energies. According to the calculated

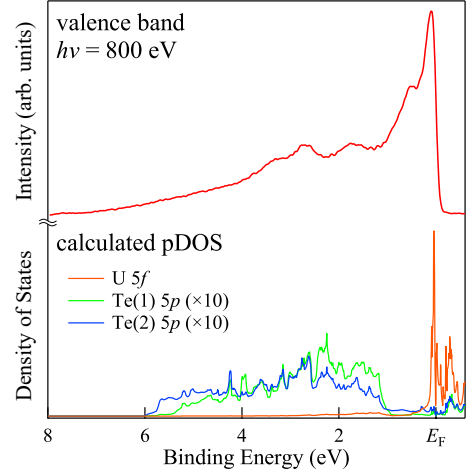


Fig. 3. Valence band spectrum of UTe_2 measured at $h\nu = 800$ eV, and the theoretical U $5f$ and Te $5p$ pDOS obtained from the band structure calculations.

photoionization cross sections of the atomic orbitals,¹⁰⁾ the contribution from the U $5f$ states is dominant in this photon energy range. The second largest contribution is that from the Te $5p$ state, the cross-section of which is about 15 % that of the U $5f$ state. Thus, the Te $5p$ state should show a tiny contribution to the spectrum. The U $5f$ and Te $5p$ pDOS obtained from the band structure calculations are also presented in the bottom of the figure. Note that the Te $5p$ pDOS are ten times enhanced in the figure. The sharp peak structure just below E_F in the experimental spectrum seems to correspond to the calculated U $5f$ pDOS, but the spectrum is much broader than the calculated U $5f$ pDOS. A shoulder structure exists at $E_B \sim 0.5$ eV and the spectral intensities at $E_B = 1-6$ eV, which should be contributions from the Te $5p$ states, are enhanced in the spectrum.

To further clarify the energy distribution of the U $5f$ state in the valence band, U $4d$ - $5f$ RPES³⁾ was applied to UTe_2 , and the results are summarized in Fig. 4. The top and left panels in Fig. 4 (a) represent the U $4d_{5/2}$ X-ray absorption spectroscopy (XAS) spectrum and photoemission spectrum measured at $h\nu = 725$ eV, respectively. The XAS spectrum has a maximum at $h\nu = 736$ eV and the spectrum measured at $h\nu = 725$ eV corresponds to the complete off-resonant condition. The density plot in the center of Fig. 4 (a) represents the difference between the spectrum measured at $h\nu = 725$ eV and that measured at each photon energy, and all of the spectra were normalized to the maximum of the spectrum measured at $h\nu = 725$ eV.

As the photon energy approaches the U $4d_{5/2}$ absorption edge, the spectra exhibit a clear enhancement, with noticeable dependence on the binding energy. This enhancement was categorized into three binding-energy regions, A, B, and C as shown in Fig. 4 (a). In binding energy region A ($E_B \lesssim 0.2$ eV), the sharp peak just below E_F exhibits a strong enhancement at the absorption edge. This is the common struc-

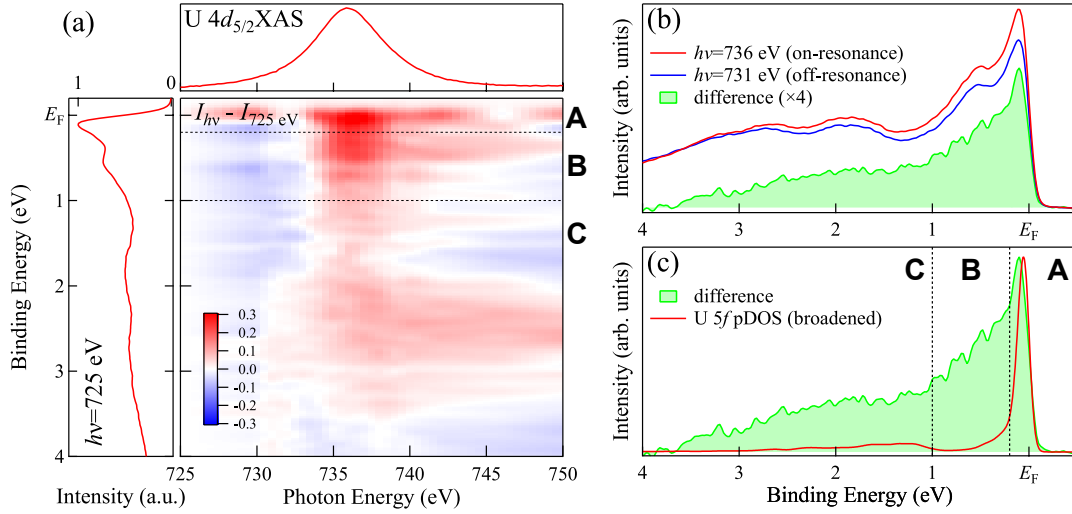


Fig. 4. RPES spectra of UTe_2 . (a) Density plot of RPES spectra together with the U $4d_{5/2}$ XAS spectrum. (b) On- and off-resonance spectra measured at $h\nu = 736$ and 731 eV, respectively, and the corresponding difference spectrum. (c) Comparison of the difference spectrum and the calculated U $5f$ pDOS.

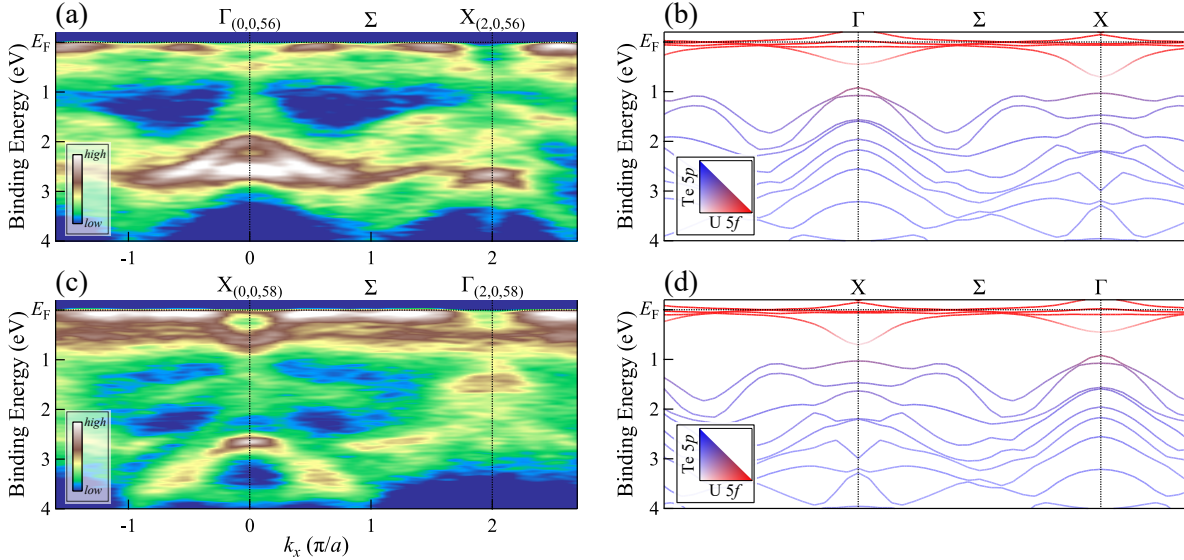


Fig. 5. ARPES spectra of UTe_2 , together with the corresponding results of the band structure calculations. (a) ARPES spectra measured along the $\Gamma_{(0,0,56)}$ – (Σ) – $X_{(2,0,56)}$ high-symmetry line. (b) The corresponding calculated band structure. The color coding represents the contribution from the U $5f$ states. (c) ARPES spectra measured along the $X_{(0,0,58)}$ – (Σ) – $\Gamma_{(2,0,58)}$ high-symmetry line. (d) Corresponding calculated band structure and the simulated ARPES spectra.

ture of itinerant U $5f$ compounds, which originates from itinerant quasi-particle bands. In the binding energy region B ($0.2 \lesssim E_B \lesssim 1.0$), there are other independent enhancements. The nature of these enhancements is very similar to the one observed in the same binding energy region of the RPES spectra of UPd_2Al_2 ³⁾ which is due to the contribution from the incoherent peak originating from electron correlation effects. The similarities in the shape and binding energy suggest that there is an incoherent peak in UTe_2 . Surprisingly, in binding energy region C ($1.0 \lesssim E_B \lesssim 3.5$), where the contributions from the Te $5p$ states are dominant in the band structure calculations, the RPES spectra exhibit weak enhancement. This

means that there is a finite contribution from the U $5f$ states in this binding energy region.

Figure 4 (b) shows the on-resonance ($h\nu = 736$ eV) and off-resonance ($h\nu = 731$ eV) spectra, along with the corresponding difference spectrum. The shape of the difference spectrum is similar to those of the valence band spectra of itinerant uranium compounds such as UAl_3 ,³⁾ but its tail persists until a much higher binding energy. The difference spectrum is compared with the calculated U $5f$ pDOS in Fig. 4 (c). The red curve represents the U $5f$ pDOS obtained from the band structure calculations, which were multiplied by the Fermi–Dirac function and broadened by the instrumental en-

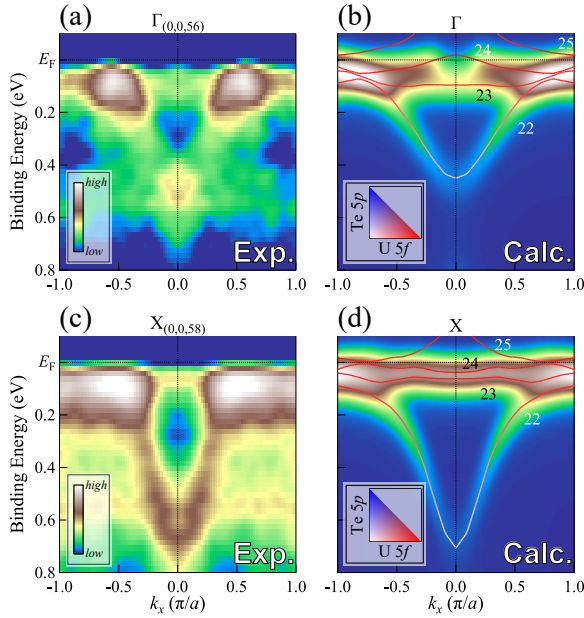


Fig. 6. Magnified ARPES spectra and the corresponding results of the band structure calculations. (a) ARPES spectra recorded around the $\Gamma_{(0,0,56)}$ point. (b) Simulation of the ARPES spectra based on the band structure calculations. (c) Same as (a) but around the $X_{(0,0,58)}$ point. (d) Same as (b) but around the X point.

energy resolution to simulate the experimental U 5*f* difference spectrum. The difference spectrum is much broader than the calculated U 5*f* pDOS. As can be seen in the resonant enhancement shown in Fig 4 (a), there are two different contributions to the broadening. In region B, there is the incoherent peak with a dominant contribution from the U 5*f* state. In region C, the finite U 5*f* contribution is admixed into the Te 5*p* band, which is not predicted by the band structure calculations. These results suggest that the U 5*f* states in UTe₂ are itinerant in nature, but there are some deviations from the simple itinerant description of the U 5*f* states.

Figure 5 (a) shows the ARPES spectra of UTe₂ measured along the $\Gamma_{(0,0,56)}-\Sigma-\Gamma_{(2,0,58)}$ high-symmetry line. Here the denotation of the point represents the location of the momentum space in the units of $\pi/a = 0.7550 [\text{\AA}^{-1}]$, $0.5131 [\text{\AA}^{-1}]$, and $\pi/c = 0.2251 [\text{\AA}^{-1}]$ for the k_x , k_y , and k_z directions, respectively (See Fig. 7 (a)). The spectra correspond to the ARPES scan with $h\nu \sim 580$ eV. The weakly dispersive features in the vicinity of E_F are quasi-particle bands with dominant contributions from the U 5*f* states. Their intensities have momentum dependence in the very vicinity of E_F , suggesting that the quasi-particle bands might form Fermi surfaces. Meanwhile, the dispersive bands at higher binding energies ($E_B \gtrsim 1$ eV) are bands with dominant contributions from the Te 5*p* states, although there are finite admixtures from the U 5*f* states, as can be seen from the RPES spectra. Figure 5 (b) shows the corresponding calculated band structure. The color coding of the bands represents the projection of the contributions from the U 5*f* and Te 5*p* states. Generally, the

bands in $E_B \lesssim 1$ eV and $E_B \gtrsim 1$ eV have dominant contributions from the U 5*f* state and the Te 5*p* states, respectively. Although each of the band is not clearly resolved in the experimental ARPES spectra, their overall structure can be mostly explained by the calculated bands. For example, the inverted parabolic dispersions around the Γ and X points in the binding energy of $E_B \gtrsim 1$ eV correspond well to the calculated bands located at the same binding energies. In addition, the less-dispersive features just below E_F also coincide with the calculated bands that have dominant contributions from the U 5*f* state, the details of which are discussed later. Figures 5 (c) and (d) show the ARPES spectra measured along the $X_{(0,0,58)}-\Sigma-\Gamma_{(2,0,58)}$ high-symmetry line and the corresponding calculated band structure, respectively. The spectra correspond to the ARPES scan with $h\nu \sim 620$ eV. The essential structure of the spectra is very similar to that measured along the $\Gamma_{(0,0,56)}-\Sigma-X_{(2,0,56)}$ high-symmetry line, but the intensities of the dispersions are different due to the momentum matrix element effect. The different appearance of the spectra makes it further possible to follow the energy dispersions. In particular, the intensity around the X point is more enhanced. As in the case of the $\Gamma_{(0,0,56)}-\Sigma-X_{(2,0,56)}$ high-symmetry line shown in Fig. 5 (a), the overall structure of the ARPES spectra can be mostly explained by the calculated bands.

Figure 6 shows magnified regions of the ARPES spectra in the vicinity of E_F and the simulation of the ARPES spectra based on the band structure calculations. In the simulation, the following factors were taken into account: the broadening along the k_z direction due to the finite escape depth of the photoelectrons, the lifetime broadening of the photohole, the photoionization cross sections of the orbitals, and the energy resolution and angular resolution of the photoelectron analyzer, the details of which are described in Ref. 11. The experimental ARPES spectra were symmetrized relative to the high-symmetry points (Γ or X) to obtain better statistics. Figure 6 (a) and (b) show the ARPES spectra and the results of the simulation around the Γ point, respectively. The experimentally-observed parabolic energy dispersion corresponds well to that of the calculated band 22. Meanwhile, the correspondences of the calculated bands 23–25 to the experimental spectra were not clear due to their very narrow dispersive natures, but the intensity maps show some similarity between the experimental data and calculations. On the other hand, the non-dispersive feature at $E_B = 0.5-0.6$ eV does not have a corresponding band and is considered to be the contribution from the incoherent peak observed in the RPES spectra. The situation is very similar to the case around the X point as shown in Figs. 6 (c) and (d). Band 22 is in good agreement well with the experimental spectra and the intensity maps in the vicinity of E_F are similar in both the experimental data and the calculations, although each band was not resolved. Besides this, the non-dispersive feature at $E_B \sim 0.5-0.6$ eV does not have a corresponding band in the calculations as in the case around the Γ point. Accordingly, it was found that the electronic structure in the vicinity of E_F is similar to that of the band structure calculations although the details of the Fermi

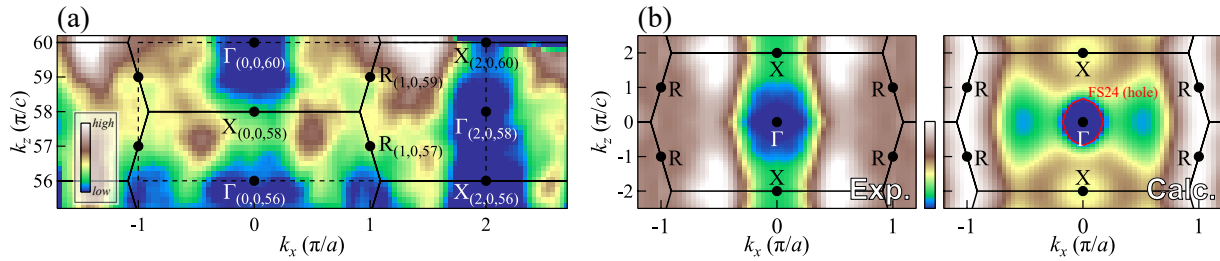


Fig. 7. Fermi surfaces of UTe_2 obtained by photon energy scanning of the ARPES measurements, together with the corresponding band structure calculation results. (a) Fermi surfaces of UTe_2 obtained by integrating the ARPES spectra measured at $h\nu = 655\text{--}745$ eV over 100 meV at E_F . (b) Symmetrized and folded Fermi surface map within the $k_x\text{--}k_z$ plane and the simulated Fermi surface map with the calculated Fermi surface.

surface topology were not resolved experimentally. In addition, an incoherent peak was observed at $E_B \sim 0.5 - 0.6$ eV in the ARPES spectra, which cannot be explained by the band structure calculations. Note that the renormalization of bands should be significant only in the very vicinity of E_F where the contributions from the U $5f$ states are enhanced.

To further understand the electronic structure in the vicinity of E_F , we discuss the Fermi surface map of UTe_2 . Figure 7 (a) shows the Fermi surface map within the $k_x\text{--}k_z$ plane obtained by integrating the ARPES spectra over 100 meV at E_F . Note that the locations with the same symmetry in the Brillouin zone but different values of k_x and k_z have different profiles. The different appearances are due to the momentum matrix element effect as has already been mentioned. To avoid this effect as much as possible, the Fermi surface map was symmetrized and folded within the momentum region within $k_x = -1 - 2(\pi/a)$ and $k_z = 56 - 60(\pi/c)$ as indicates by the dashed lines in Fig. 7 (a). Figure 7 (b) shows a comparison between the symmetrized and folded Fermi surface map and the simulated Fermi surface map based on the band structure calculations. Within this high-symmetry plane, the calculations predict a hole pocket formed by band 24. Although the Fermi surface maps have different intensity distributions in the experimental data and calculations, some similarities between them can be recognized. In particular, the intensity around the Γ point is reduced in both the experimental data and the calculations, and their shapes are similar to each other. In addition, the intensities around the R point are enhanced in both the experimental data and the calculations although their shapes are somewhat different. These similarities in the Fermi surface map as well as the bands in the vicinity of E_F between the experimental data and calculations suggest that the essential structure of the Fermi surface should not be so different from the band structure calculation although their topologies were not directly determined.

In summary, U $4d\text{--}5f$ RPES and ARPES were applied to UTe_2 . The overall band structure of UTe_2 can be described by band structure calculations, although there is the non-dispersive incoherent band at $E_B = 0.5 - 0.6$ eV originated from the strong electron correlation effects. The topology of the Fermi surface was not resolved experimentally due to the very narrow nature of the bands in the vicinity of E_F , but sim-

ilar spectral profiles were observed in the experimental data and the band structure calculation. Thus, the electronic structure of UTe_2 can be described by taking into account the electron correlation effect to the itinerant U $5f$ model, and the superconductivity in UTe_2 is mediated by the heavy quasi-particles. On the other hand, the U $5f$ states are mixed with the Te $5p$ bands distributed at deeper binding energies, the behavior of which could not be explained by the band structure calculations. The origin of the anomalous admixture is not understood at present.

The experiment was performed under Proposal Nos 2019A3811 at SPring-8 BL23SU. The present work was financially supported by JSPS KAKENHI Grant Numbers JP15H05882, JP15H05884, JP15H05745, JP15K21732, JP16H01084, JP16H04006, JP18K03553, and JP19H00646.

- 1) S. Ran, C. Eckberg, Q.-P. Ding, Y. Furukawa, T. Metz, S. R. Saha, I.-L. Liu, M. Zic, H. Kim, J. Paglione, and N. P. Butch: *Science* **365** (2019) 684.
- 2) D. Aoki, A. Nakamura, F. Honda, D. Li, Y. Homma, Y. Shimizu, Y. J. Sato, G. Knebel, J.-P. Brison, A. Pourret, D. Braithwaite, G. Lapertot, Q. Niu, M. Vališka, H. Harima, and J. Flouquet: *J. Phys. Soc. Jpn.* **88** (2019) 043702.
- 3) S.-i. Fujimori, M. Kobata, Y. Takeda, T. Okane, Y. Saitoh, A. Fujimori, H. Yamagami, Y. Haga, E. Yamamoto, and Y. Ōnuki: *Phys. Rev. B* **99** (2019) 035109.
- 4) S.-i. Fujimori, Y. Takeda, T. Okane, Y. Saitoh, A. Fujimori, H. Yamagami, Y. Haga, E. Yamamoto, and Y. Ōnuki: *J. Phys. Soc. Jpn.* **85** (2016) 062001.
- 5) Y. Saitoh, Y. Fukuda, Y. Takeda, H. Yamagami, S. Takahashi, Y. Asano, T. Hara, K. Shirasawa, M. Takeuchi, T. Tanaka, and H. Kitamura: *J. Synchrotron Rad.* **19** (2012) 388.
- 6) S. Fujimori, T. Ohkochi, I. Kawasaki, A. Yasui, Y. Takeda, T. Okane, Y. Saitoh, A. Fujimori, H. Yamagami, Y. Haga, E. Yamamoto, and Y. Ōnuki: *Phys. Rev. B* **91** (2015) 174503.
- 7) H. Yamagami: *J. Phys. Soc. Jpn.* **67** (1998) 3176.
- 8) U. von Barth and L. Hedin: *J. Phys. C: Solid State Phys.* **5** (1972) 1629.
- 9) S.-i. Fujimori, I. Kawasaki, A. Yasui, Y. Takeda, T. Okane, Y. Saitoh, A. Fujimori, H. Yamagami, Y. Haga, E. Yamamoto, and Y. Ōnuki: *Phys. Rev. B* **89** (2014) 104518.
- 10) J. Yeh and I. Lindau: *Atomic Data and Nuclear Data Tables* **32** (1985) 1.
- 11) S. Fujimori, T. Ohkochi, T. Okane, Y. Saitoh, A. Fujimori, H. Yamagami, Y. Haga, E. Yamamoto, and Y. Ōnuki: *Phys. Rev. B* **86** (2012) 235108.